Visual Neuroscience (2008), Page 1 of 14. Printed in the USA.

doi:10.1017/S095252380808067X

The maintained discharge of rat retinal ganglion cells

DANIEL K. FREEMAN, WALTER F. HEINE, AND CHRISTOPHER L. PASSAGLIA

Department of Biomedical Engineering, Boston University, Boston, Massachusetts

(RECEIVED February 19, 2008; ACCEPTED April 21, 2008)

Abstract

Action potentials were recorded from rat retinal ganglion cell fibers in the presence of a uniform field, and the maintained discharge pattern was characterized. Spike trains recorded under ketamine–xylazine anesthesia were generally stationary, while those recorded under urethane anesthesia often showed slow, undriven, quasiperiodic fluctuations in firing rate. In light of these nonstationarities, interspike interval distributions and power spectral densities are reported for data collected primarily under ketamine–xylazine. The majority of cells had multimodal interval distributions, with the first peak in the range of 25.0–38.5 ms and the subsequent peaks occurring at integer multiples of the first peak. Cells with unimodal distributions were fit well by a gamma distribution function. Interval and spike count statistics showed that ON cells tended to fire faster than OFF cells and that cells with higher rates fired in a more regular manner, with the coefficient of variation covering a wide range of values across all cells (0.43–0.97). Both ON and OFF cells show serial correlations between adjacent interspike intervals, while ON cells also showed second-order correlations. Cells with multimodal interval distribution showed a strong peak at high frequencies in the power spectra in the range of 28.9–41.4 Hz. Oscillations were present under both anesthetic conditions and persisted in the dark at a slightly lower frequency, implying that the oscillations are generated independent of any light stimulus but can be modulated by light level. The oscillation frequency varied slightly between cells of the same type and in the same eye, suggesting that multiple oscillatory generating mechanisms exist within the retina. Cells with high-frequency oscillations were described well by an integrate-and-fire model with the input consisting of Gaussian noise plus a sinusoid where the phase was jittered randomly to account for the bandwidth present in the oscillations.

Keywords: Maintained discharge, Interval distributions, Power spectra, Serial correlations, Oscillations

Introduction

Information about the visual world is transmitted to the brain in the form of sequences of action potentials in retinal ganglion cells that make up the optic nerve. In the presence of steady uniform illumination, most ganglion cells in the mammalian retina continually fire action potentials in an irregular pattern referred to as the maintained discharge (Kuffler et al, 1957; Rodieck, 1967). Any further stimulus must produce a change in ganglion cell firing pattern that is distinct from this background noise in order for an animal to detect it, motivating the need for a quantitative description of discharge noise statistics. To date, the maintained discharge has been analyzed for several species, including cat (Barlow & Levick, 1969; Frishman & Levine, 1983; Troy & Robson, 1992), primate (Troy & Lee, 1994), and goldfish (Levine & Shefner, 1977). Here we provide the first detailed report on the maintained discharge properties of rat retinal ganglion cells.

A fundamental aspect of any description of spike train statistics is stationarity. Most studies on anesthetized animals report that the maintained discharge statistics are constant throughout the duration of a recording, presumably indicative of a stable healthy cell. Several studies though have cited a phenomenon in which ganglion cell spike rate waxes and wanes in time (Kuffler et al. 1957; Levick & Williams 1964; Rodieck & Smith, 1966; Barlow & Levick, 1969). The undulations in activity can be large in amplitude and irregular in frequency or highly rhythmic, with periods of seconds to many minutes (Rodieck & Smith, 1966). They presumably contribute to the power law growth in discharge noise variance seen at long timescales (Teich et al., 1997). The source of the phenomenon has yet to be determined. Experimental variables, such as blood pressure, oxygenation, temperature, anesthetic, and illumination, have all been manipulated, and only the latter was found to affect rhythms in the maintained discharge. However, we find that rat ganglion cell spike trains are reasonably stationary for certain anesthetics but not for others commonly used in vision experiments. The differences in anesthetic effect may provide insight into the physiological or pathological origin of the rhythms.

Another important descriptor of the maintained discharge is the distribution of intervals between spikes and the extent to which the intervals depend on the spike history of the cell. Spike trains generated by a renewal process have interspike intervals that are statistically independent, which means that they are completely described by the probability density function from which the intervals are drawn. Cat and primate retinal ganglion cell spike trains do not strictly fall within the definition of a renewal process because slight negative correlations exist between adjacent intervals (Kuffler et al., 1957; Rodieck, 1967; Troy & Robson, 1992; Troy & Lee, 1994), whereby short intervals tend to be followed by long

Address correspondence and reprint requests to: Daniel K. Freeman, Department of Biomedical Engineering, Boston University, 24 Cummington Street, Room 232, Boston, MA 02215. E-mail: dfreeman@bu.edu

intervals and vice versa. However, to a good approximation, they can be described by a renewal process with gamma-distributed interspike intervals and power spectra. We find that this description also applies to rat ganglion cell spike trains, with the caveat that most cells show a propensity for fast oscillatory discharge, which we define as oscillations in the spike train at relatively high frequencies, beyond which a typical ganglion cell can resolve in response to a light stimulus.

One of the goals in characterizing the statistical properties of the maintained discharge is to gain insight into the retinal mechanisms that generate the discharge noise and its defining features. Possible sources of spike train irregularities include phototransduction noise (Schneeweis & Schnapf, 1999), synaptic noise (Demb et al., 2004; Freed, 2005), and stimulus noise due to the stochastic nature of photon arrival (Hecht et al., 1942). Simulations have shown that a simple integrate-and-fire model with a white noise input produces gamma-distributed interspike intervals and power spectra like those of mammalian retinal ganglion cells (Levine, 1991; Passaglia & Troy, 2004). This model is not sufficient for describing rat ganglion cell spike trains, however, because we find that most cells have multimodal interval distributions. Similar-shaped distributions have been reported in goldfish (Levine & Shefner, 1977) and occasionally in cat (Ogawa et al., 1966; Rodieck, 1967). We show that the model can capture the maintained discharge of rat ganglion cells if it is modified to include a high-frequency oscillatory input.

Materials and methods

Physiological preparation

Anesthesia was induced in 30 adult Brown Norway rats using one of the following protocols: (1) an intraperitoneal (IP) injection of urethane (1.8 g/kg), (2) an IP injection of a urethane (500 mg/kg) and chloralose (800 mg/kg) mixture, (3) an IP injection of ketamine hydrochloride (70 mg/kg) and xylazine (2.3 mg/kg) mixture, and (4) 1%–2% isoflurane (flowmeter set to 1 l/min). Urethane has a long-lasting effect and rarely needed supplemental doses. Ketamine hydrochloride and xylazine were supplemented intravenously at 60 and 2 mg/kg/h, respectively. The urethane–chloralose mixture was supplemented intravenously as needed. Preparatory surgery included the insertion of tubing into the femoral vein for drug delivery and, in some experiments, into the femoral artery for measuring blood pressure. Heart rate was monitored with an electrocardiogram and body temperature maintained near 37.0°C with a heated blanket. An intramuscular injection of dexamethasone (1 mg) was given to reduce brain pulsations. The pupil was dilated with atropine sulfate (1%), and a clear contact lens was placed over the eye to protect from drying. The animal was placed in a stereotaxic apparatus, and the skull was surgically exposed. Hydrogen peroxide was used to clean the skull surface and allowed identification and stereotaxic calibration to bregma and lambda. A 5-mm hole was drilled in the skull either directly over bregma for optic chiasm recordings or 1.5 mm lateral to bregma for optic tract recordings. All experimental procedures were approved by Boston University Animal Care and Use Committee.

Recording and visual stimulation

Custom-made tungsten-in-glass microelectrodes were used to record extracellularly from retinal ganglion cell axons (Levick, 1972). Impedances in the range of 0.7 to 1.2 MΩ (IMP-2 impedance tester, 30 nA current, 1 kHz frequency; Bak Electronics, Rockville, MD) were sufficient to both locate visual cells and isolate single units. Electrodes were advanced into the brain either 0.5 mm anterior to bregma (optic chiasm) or 1.5 mm lateral to bregma (optic tract) through a protective guide tube. A video monitor (Multiscan 17se, 40.4 × 30.2 cm; Sony New York, NY) was placed on a moveable platform that allowed rotational movement of the screen about a 16-cm arc from the eye. The monitor was positioned on its side to maximize the vertical extent of the screen. The frame rate of the monitor was 100 Hz (noninterlaced), and the mean luminance was 26 cd/m^2, which is in the photopic range for rat (Cicerone & Green, 1980). Custom software controlled the monitor output using Matlab, LabView, and the Psychophysics Toolbox (Brainard, 1997). The monitor was gamma corrected as to linearize the input–output relationship governing monitor intensity. Upon isolation of a single cell, its receptive field was located and centered on the screen. Spike times were recorded with a digital spike discriminator sampling at 10 kHz (Acquisition Processor Module; FHC Inc., Bowdoin, ME).

Cells were first determined as being either ON or OFF based on their response to handheld wands. Cells were further categorized using the classification scheme in cat where X and Y cells respond briskly when stimulated (Cleland & Levick, 1974) and W cells generally respond in a more sluggish manner (Troy & Shou, 2002). W cells were encountered but were recorded too infrequently for inclusion. Differentiating X and Y cells was done using a sinusoidal grating of high spatial frequency that reversed sinusoidally in contrast at 2 Hz. Y-cell responses have a strong second harmonic (F2) component for gratings whose spatial frequency is too high to produce a modulated response (F1) from the center mechanism (Hochstein & Shapley, 1976). Thus, for spatial frequency just beyond the resolution of the center mechanism, Y cells gave F2 > F1 and X cells did not. The maintained discharge was recorded for 2–5 min for each cell, with an average number of total spikes per cell of 2775 for ON cells and 808 for OFF cells.

Tests of stationarity

In order to determine whether the statistics of the maintained discharge were constant throughout the duration of a given record, the Run Test for stationarity was used (Bendat & Piersol, 1986). This is a nonparametric procedure and thus makes no assumptions about the probability distribution of the data. Negative serial correlations between adjacent intervals might be expected given the findings in other animals (Troy & Robson, 1992; Troy & Lee, 1994), so the data were segmented into groups of 8, 16, 32, or 64 intervals to minimize the influence of correlations on the stationarity test. By using segments that contain various numbers of intervals, the test probes for nonstationarities that occur on differing timescales. For a spike train consisting of N segments, where the duration of each segment is given by the random variable x, the Run Test is constructed by taking the sequence of observed values $x_i = 1, 2, 3, \ldots N$ and classifying each value as being above or below the median, x_m. Observations where $x_i \geq x_m$ are assigned 1 and values where $x_i < x_m$ are assigned 0. Thus, an example of a set of observations would be 011000110111. The total number of clusters of 0s or 1s is defined as the number of runs, r, where $r = 6$ in the example shown. For the case where x is generated by a stationary process, the sequence of N observations is drawn from a probability distribution that is unchanging in time, which will result in mean and variance of the random variable, r,

that are known quantities that can be calculated (Bendat & Piersol, 1986) and come out to be

$$\mu_r = \frac{N}{2} + 1; \quad \sigma_r^2 = \frac{N(N-2)}{4(N-1)}.$$

To facilitate interpretation of the test result, we map the random variable r onto a new random variable R, which has a zero-mean, unit-variance distribution and is referred to as the run score. The mapping is performed by subtracting off the mean and dividing by the standard deviation of r. The distribution function of R is undefined, but for large values of N, it follows a normal distribution to a good approximation. The end result is that stationary spike trains should give R near zero, and significant deviations from zero indicate nonstationarities.

Interspike interval and spike count statistics

The statistics of the spike train were analyzed in two ways. First, the lengths of time between adjacent spikes for all spikes in a given record were collected, and a histogram of the frequency of occurrence of different interspike intervals was constructed. The standard deviation of interspike intervals divided by the mean interspike interval is called the coefficient of variation (CV) and was used to quantify the irregularity of the spike train. The second method was to consider the number of spikes that occur in 1-s windows over the duration of the spike train. The average number of spikes in a given window, or spike count, and the standard deviation of the spike count were computed.

Serial correlation coefficients

Correlations between interspike intervals were investigated using the method of Goldberg et al. (1964). Records were divided up into segments of 20 intervals, and the correlation between a given interval, τ_i, and $(i + k)$th interval, τ_{i+k}, was computed. The kth serial correlation between these two intervals, s_k, is defined as

$$s_k = \frac{N\sum_{i=1}^{N}\tau_i\tau_{i+k} - \sum_{i=1}^{N}\tau_i\sum_{i=1}^{N}\tau_{i+k}}{\sqrt{\left[N\sum_{i=1}^{N}\tau_i^2 - \left(\sum_{i=1}^{N}\tau_i\right)^2\right]\left[N\sum_{i=1}^{N}\tau_{i+k}^2 - \left(\sum_{i=1}^{N}\tau_{i+k}\right)^2\right]}} - \frac{k-N}{N(N-1)},$$

where $N = 20$. The first term is the sample correlation coefficient, while the second term is a correction factor that was introduced so that s_k would be zero when there is no correlation between intervals. If, for example, a short interval tends to be followed by a long interval, then the first correlation coefficient will tend to be negative. The second correlation coefficient would be a measure of how correlated an interval is with two intervals ahead and so on with higher order coefficients.

Power spectral densities

The power spectral density provides information on temporal structure present in a spike train, expressing its output as a function of frequency. Power spectra were computed by first binning the spike train at 5 ms and counting the number of spikes in each window and dividing by the bin size to get units that are impulses per second. This response vector was segmented into durations of 5.12 s, and each segment was processed using the fast Fourier transform function in Matlab. The Fourier coefficients of each segment were then squared and summed to give the average power spectral densities. Segmenting the spike trains helps reduce uncertainty in power spectral estimates (Marmarelis & Marmarelis, 1978). The spike trains were binned at 5 ms because smaller bin sizes did not reveal any new or significant features above 100 Hz.

Results

Stationarity

The maintained discharge of 143 cells was analyzed for stationarity. In general, cells under urethane anesthesia exhibited periods of instability, wherein the firing rate fluctuated significantly even though the receptive field was steadily and uniformly illuminated ($n = 56$). The fluctuations were sometimes periodic (Fig. 1A), but more often they were irregular and unpredictable (Fig. 1B). Similar behavior was observed in cells under urethane–chloralose ($n = 2$) and isoflurane anesthesia ($n = 4$) (Fig. 1C, 1D). In contrast, cells under ketamine–xylazine anesthesia were very stable ($n = 81$) (Fig. 1E, 1F).

Visual inspection of the spike rate record was often sufficient for identifying nonstationary behavior. To confirm this quantitatively, a Run Test was performed on 8, 16, 32, and 64 segment intervals, and the results are given in Table 1. The run score is a zero-mean, unit-variance, normally distributed variable, where significant deviations from zero indicate nonstationarity (see Methods). Averaging across all cells, the run score was significantly different from zero for all interval sizes under urethane anesthesia but not under ketamine–xylazine anesthesia ($P < 0.05$). Rat ganglion cells under urethane or isoflurane anesthesia were thus subjected to a slow time-varying input that was absent under ketamine–xylazine anesthesia. X and Y cells were similarly affected by urethane anesthesia, both displaying nonstationarities and having run scores that were not significantly different ($P < 0.05$). Consistent with this finding, waxing and waning has not been observed in other vision experiments that used ketamine–xylazine on rats (Girman & Lund, 2007), mice (Sagdullaev & McCall, 2005), or cats (Haider et al., 2007). However, it is unclear why the waxing and waning of firing rate was not reported in prior vision experiments that used urethane on rats (Brown & Rojas, 1965; Powers & Green, 1978; Cicerone & Green, 1980).

Since our goal was to characterize the maintained discharge properties of ganglion cells that are in a stable condition, the subsequent analysis in this report considers data collected under ketamine–xylazine anesthesia. A total of 90 retinal ganglion cells were recorded. The number of each cell type is given along with the mean and standard deviation of the firing rate: 38 ON-X cells (12.6 ± 6.4 impulses/s), 19 ON-Y cells (15.5 ± 5.9 impulses/s), 21 OFF-X cells (3.1 ± 3.5 impulses/s), and 12 OFF-Y cells (3.4 ± 3.5 impulses/s). The mean rate was not significantly different between ON-X and ON-Y cells or between OFF-X and OFF-Y cells, but it was different between ON and OFF cells ($P < 0.05$). A total of eight OFF-X and one OFF-Y cells had close to zero maintained discharge and fired only in response to dynamic visual stimulation. These cells were not included in the analysis.

Interspike interval distributions

Previous reports on the maintained discharge of cat and primate retinal ganglion cells have interspike interval distributions that are

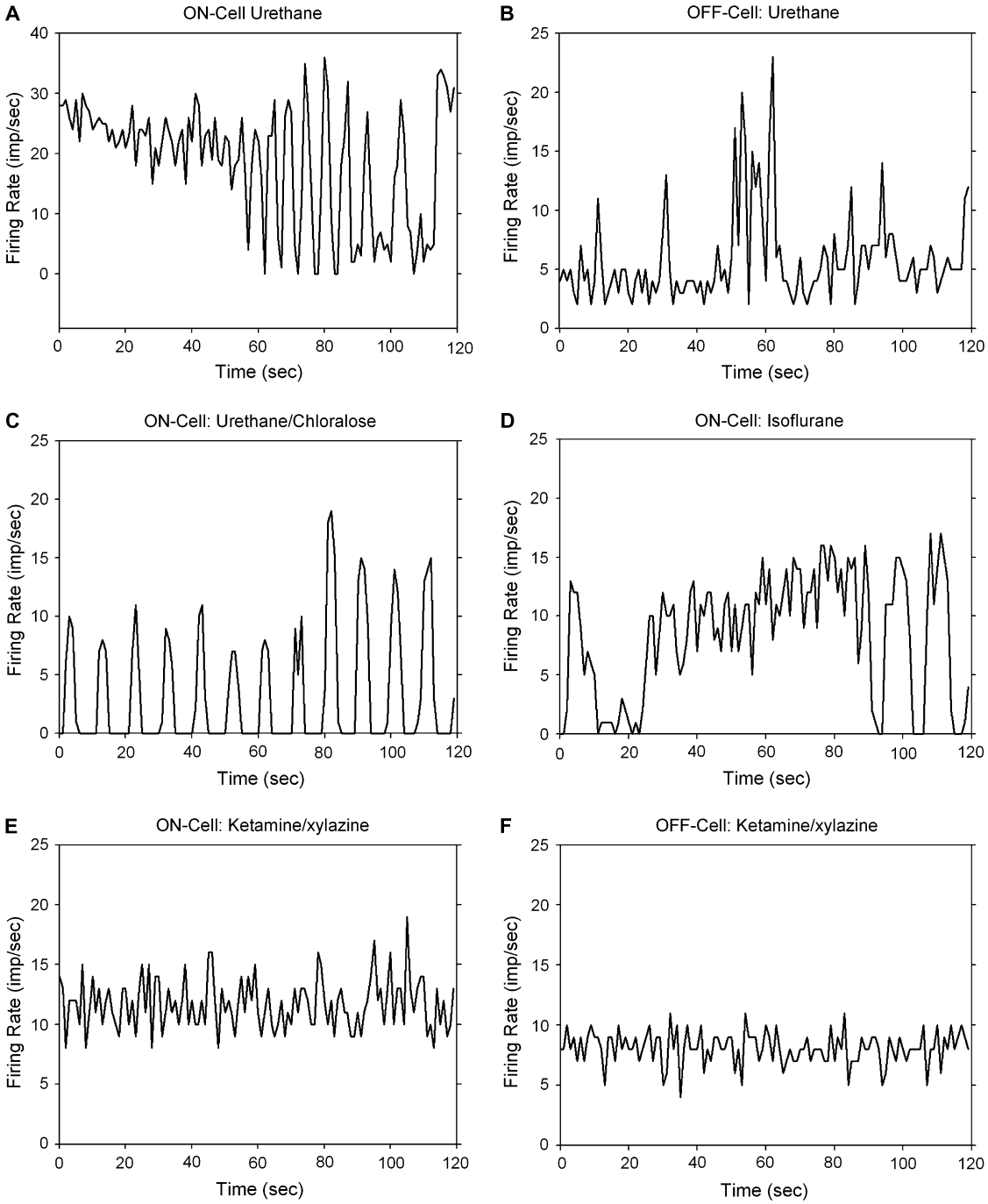

Fig. 1. Effects of anesthesia on the maintained discharge, showing the firing rate over a 2-min period (bin size = 1 s). The average run score, *R*, is given and was computed across 8, 16, 32, and 64 interval sets for each record. Examples under urethane anesthesia for an ON cell ($R = -1.12$) (**A**) with periodic fluctuations in rate and an OFF cell ($R = -6.99$) (**B**) showing random fluctuations in rate. Urethane–chloralose ($R = -4.10$) (**C**) and isoflurane ($R = 1.79$) (**D**) anesthesia showed quasiperiodic fluctuations in rate similar to that seen under urethane alone. Ketamine–xylazine anesthesia gave stationary discharges, with examples from a typical ON cell ($R = 0.06$) (**E**) and OFF cell ($R = 0.12$) (**F**).

fit well by a gamma distribution function (Troy & Robson, 1992; Troy & Lee, 1994). The majority of cells that we encountered in rat, however, had multimodal interval distributions (29 of 38 ON-X, 15 of 19 ON-Y, 8 of 13 OFF-X, and 7 of 11 OFF-Y). The modes were all located at integer multiples of the first mode, which tended to be around 30 ms, and the initial modes were most pronounced (Fig. 2A–2D). Physiologically, this means that when a cell fires a spike, it has a strong tendency to fire another ~30 ms later, but it sometimes fails to fire a spike then. When that happens, the cell tends to fire 60 ms later or 90 ms later and so on. Hence, the cells show fast oscillatory discharges. The mean and standard deviation of the preferred interval for each cell type were estimated from the local maximum of the first mode of the interspike interval distribution. The results were 29.6 ± 2.7 ms for

Table 1. *Run Test for stationarity results under ketamine–xylazine anesthesia and urethane anesthesia**

Intervals	Ketamine–xylazine	Urethane
8	0.239 (1.39)	−2.82 (4.23)
16	−0.287 (1.43)	−2.60 (3.51)
32	−0.497 (1.34)	−2.03 (2.63)
64	−0.823 (1.24)	−1.99 (2.08)

*The mean and standard deviation (in parentheses) of the run score for 56 cells under urethane and 81 cells under ketamine–xylazine are given for segments consisting of 8, 16, 32, and 64 intervals.

ON-X cells, 28.5 ± 3.1 ms for ON-Y cells, 31.6 ± 3.7 ms for OFF-X cells, and 32.7 ± 2.7 ms for OFF-Y cells. Interestingly, the location of the first mode was independent of the mean firing rate, as shown in Fig. 2E. Even cells with little maintained discharge tended to fire spikes in ~30-ms intervals and multiples thereof. The preferred interval of OFF cells was statistically longer than that of ON cells ($P < 0.05$), but the variability across cells was sufficient that the mechanism driving the fast oscillatory discharge could well be the same for all cell types.

There was a clear dependence of the number of modes in the interval distribution on the mean firing rate (Fig. 2F). Cells with low maintained discharge generally present the most modes. Presumably this is because the interval distributions are inherently broader for these cells, allowing for more modes to become apparent. It is likely that in the absence of the fast oscillatory discharge, the cells would have gamma-distributed intervals like in cat and primate because other cells that have unimodal interval distributions were well fit by a gamma function, as discussed later. Related to this, a common but less striking feature of interval distributions was a small bump in the range of 4–12 ms (Fig. 2A–2C). It was not always easy to detect, especially for low–mean rate cells, given the small probabilities of interval occurrence. The feature likely reflects instances in which the fast oscillatory drive on the cell is large enough to fire a pair of spikes during a cycle. The refractory period of the spiking mechanisms then combines to make this a relatively rare event.

Interval and spike count statistics

The distribution of interspike intervals in a given record provides information on the processes that underlie the generation of the maintained discharge. For cells with a lower mean firing rate, and therefore longer intervals, the variability of interval duration tended to be greater. This is illustrated in Fig. 3A, where the mean interspike interval is plotted *versus* the standard deviation of intervals for each cell. The best-fit line has a slope of 1.17 and y-intercept of -0.56 ($r = 0.997$). The near-unity slope indicates that changes in the mean interval result in approximately equal changes in the standard deviation of intervals. This, coupled with the negative intercept, also indicates that the mean interval is larger than the standard deviation of intervals. Since the slope was not exactly 1, the CV of the maintained discharge was generally greater for cells that fire at low rates (Fig. 3B). For all cells, though, the CV is less than 1, consistent with their non-Poisson interval distributions. The result is that OFF cells, on account of their higher CV, have more irregular spike trains than ON cells.

The spike count, or the number of spikes in a given time window, was also examined. It was found that cells with a higher mean spike count tended to have a larger standard deviation of counts (Fig. 3C). Expressing the relative variability as the standard deviation normalized by the mean spike count, we see that the maintained discharge becomes exponentially less variable as the mean rate increases (Fig. 3D). This is a distinctly non-Poisson feature, as the mean and variance of the spike count would be equal for a Poisson process. ON and OFF cells with similar firing rates have overlapping count and interval statistics, implying that the regularity of the maintained discharge is a reflection of the discharge rate regardless of cell polarity.

Serial correlations

In cat, it has been shown that adjacent interspike intervals are not independent in duration but are negatively correlated (Kuffler, 1957; Rodieck, 1967; Frishman & Levine, 1983; Robson & Troy, 1987; Troy & Robson, 1992). That is to say, a relatively short interval tends to be followed by a relatively long interval and vice versa. The same was true for rat retinal ganglion cells where the first correlation coefficient was negative for all cell types (Fig. 4A, 4B). The second correlation coefficient was also significantly negative for ON cells, implying that the length of a given interval will be dependent on the two previous intervals. For ON-X cells, the third coefficient was also significantly negative ($P < 0.05$).

For OFF cells, the coefficients were more variable. The first correlation coefficient, for example, spanned a wider range of values across the population of cells in spite of the narrower range of their maintained discharge rate compared to ON cells (Fig. 4C, 4D). There was a slight dependence of the first coefficient on the mean rate for OFF-X ($r = -0.65$) and ON-Y ($r = 0.63$) cells such that the adjacent intervals were more negatively correlated for the former and less so for the latter as the mean rate increased. A similar relationship was not apparent for ON-X ($r = 0.01$) or OFF-Y ($r = -0.10$) cells.

Higher order correlation coefficients were slightly positive, particularly for ON cells. The later positive coefficients could reflect a monotonic drift in their mean firing rate over time (Perkel et al., 1967), except that the stationarity tests that were performed would have revealed such trends. Instead, the later positive coefficients can be seen as a by-product of the early negative correlations.

For example, negative correlations imply that a very short interspike interval tends to be followed by longer intervals. Following these longer intervals, the cell will once again be allowed to fire at any interval size, and if this interval tends to be shorter than the mean interval, a positive correlation will result. However, the mean interval tends to be artificially large due to the presence of longer intervals caused by early negative correlations. Thus, when the cell is allowed to fire at any interval size, it tends to be shorter than the mean and positive correlations result.

Power spectral densities

The power spectrum is another useful tool for revealing temporal structure in a spike train. The general shape of the maintained discharge spectrum of rat retinal ganglion cells resembles that reported for cat and primate, where the power density is flat at low temporal frequencies and ramps up at frequencies around 10 Hz to a plateau level numerically equal to the mean firing rate (Fig. 5A–5D) (Troy & Robson, 1992; Troy & Lee, 1994). Since ON cells usually have high mean rates, most of their power density is concentrated at higher frequencies. OFF cells, on the other hand, due to their low mean rates have power density distributed more uniformly across temporal frequency.

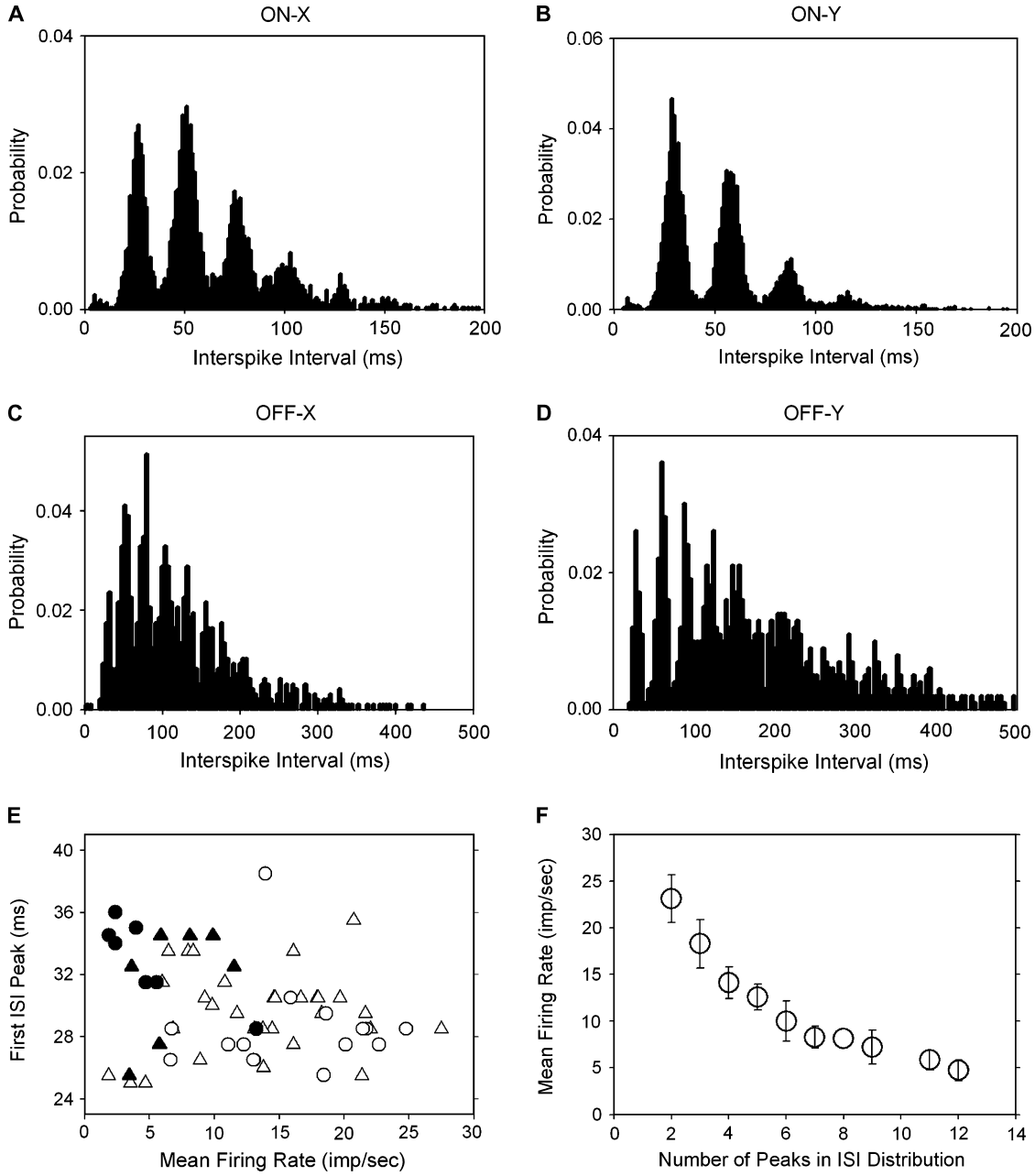

Fig. 2. Multimodal interspike interval distributions for all cell types. For ON cells (**A**, **B**), the bin size is 1 ms, and for OFF cells (**C**, **D**), the bin size is 4 ms. (**E**) The mean firing rate of each cell is plotted against the interspike interval at which the first peak occurred. (**F**) The number of peaks in each interval distribution is plotted against the mean firing rate of each cell (ON-X, open triangles; ON-Y, open circles; OFF-X, filled triangles; OFF-Y, filled circles).

Perhaps the most striking and unique feature of the power spectra of most rat ganglion cells is the large peak in the range of 20–40 Hz. The peak is indicative of fast oscillations in the maintained discharge. Within the population of recorded cells, an oscillatory peak was visible for 31 of 35 ON-X, 15 of 16 ON-Y, 8 of 13 OFF-X, and 6 of 11 OFF-Y cells. The oscillation frequency, which was defined as the point of maximal power density in the range of 20–50 Hz, was not significantly different between any two cell types ($P < 0.05$). Across all cell types, the oscillation occurred at an average frequency of 35.2 ± 3.0 Hz, well above the maintained discharge rate and temporal frequency response of a typical rat ganglion cell, which cuts off at 10–20 Hz (unpublished observations). Lowering the frame rate of the monitor from 100 to 60 Hz did not affect the power spectral densities or interval distributions ($n = 6$, not shown), implying that the oscillations were not induced by the monitor. The power spectra of many ON cells (26 of 57) contained another peak at twice the oscillation frequency (Fig. 5C). A plot of the oscillation frequency against the first mode of the interval distribution showed an inverse relationship with a unity-slope line ($r = 0.76$) (Fig. 6A). Such a relationship is expected since an oscillatory discharge produces an abundance of intervals of a certain period.

Upon zooming in, it becomes clear that the high frequency peak has considerable bandwidth (Fig. 6B), suggesting that the

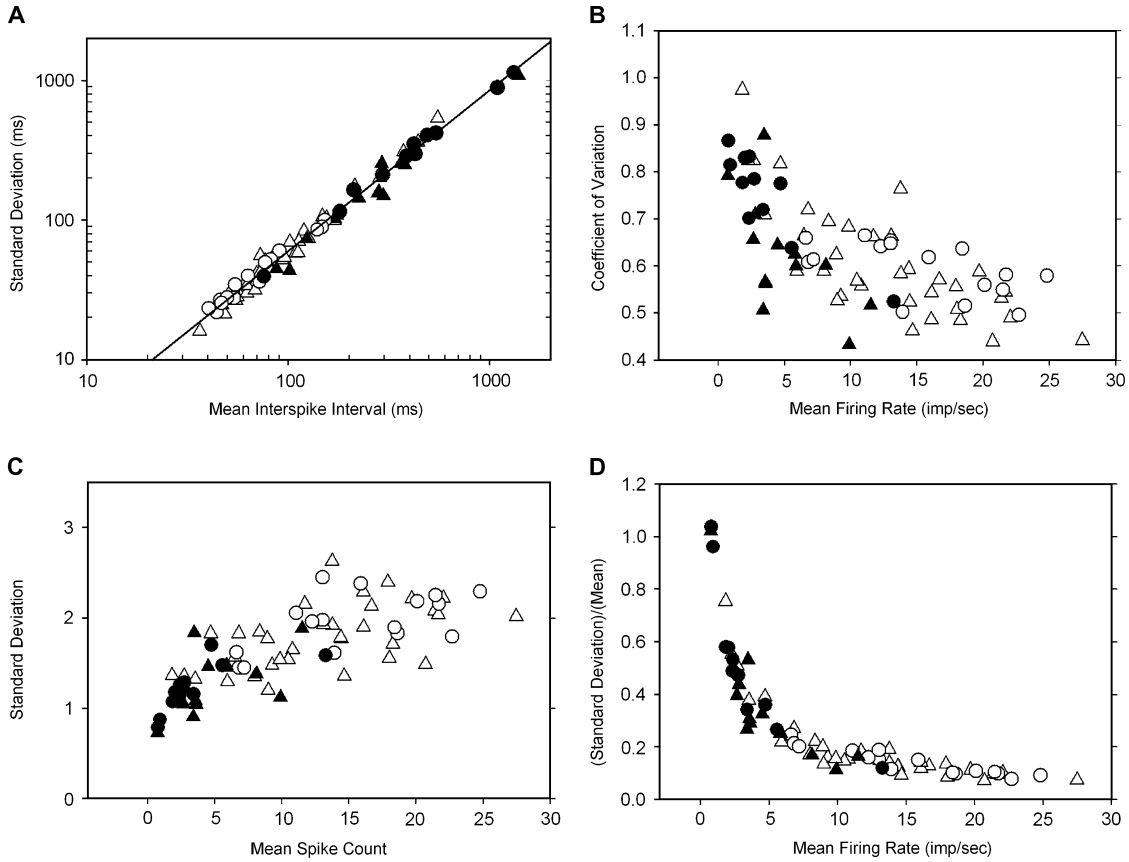

Fig. 3. Interval and spike count statistics. (**A**) The standard deviation of interspike intervals in the maintained discharge of each cell is plotted against the mean interval, where the line shown is the best fit with slope of 1.17 and y-intercept of -0.557 ($r = 0.997$). (**B**) The CV, or the standard deviation of intervals normalized by the mean interval, is plotted against the mean firing rate of each cell. (**C**, **D**) The spike count, which is the number of spikes occurring in 1-s windows, is averaged across the maintained discharge of each cell and plotted against the standard deviation (**C**) as well as the standard deviation normalized by the mean (**D**) (ON-X, open triangles; ON-Y, open circles; OFF-X, filled triangles; OFF-Y, filled circles).

oscillatory driving force on the spiking mechanism is not a pure sinusoid. Also, the three cells shown in the figure are all ON-Y cells, two of which (R94C2 and R94C6) are from the same animal and eye. This illustrates that cells of the same type within the retina can oscillate at different frequencies with various bandwidths. The amplitude of the oscillatory peak was quantified as the maximum deviation of the power density from the average power density in the range of 45–50 Hz, which is a flat region of the spectrum. The peak amplitude is an estimate of the strength of the oscillatory forces acting on the maintained discharge. There is a strong correlation between the mean firing rate of a cell and the amplitude of the peak ($r = 0.93$) (Fig. 6C), meaning that the more often a cell fires, the more oscillatory discharge its spike train has. The width of the high frequency peak was measured by fitting a Gaussian curve to it, and the standard deviation of this best-fit Gaussian is plotted against the mean rate (Fig. 6D). It is clear that there is no correlation between bandwidth and the mean firing rate ($r = -0.19$). There was also no correlation between the mean firing rate and the oscillatory frequency ($r = 0.12$) (Fig. 6E).

Effect of light level and anesthesia on fast oscillatory discharge

To determine whether the oscillatory peak was influenced by light, the maintained discharge of some ganglion cells was recorded in darkness as well as photopic illumination. Recordings in the dark were made with the stimulus monitor and room lights off with the animal behind a curtain to shield from the lights of any recording instruments. The cells were allowed several minutes to adapt when changing the light level, and in every case ($n = 9$ ON cells), the oscillations were still present in the dark. Interestingly, though, the peak frequency consistently decreased in the dark (Fig. 7A). The average frequency shift was small (2.11 ± 0.85 Hz) compared to the change in light level, but it was reproducible and statistically significant ($P < 0.05$). Cells showing multimodal interval distributions at photopic levels will also be multimodal in the dark (Fig. 7B), with the peaks shifted slightly toward longer intervals. Therefore, the mechanism responsible for high-frequency oscillations in the maintained discharge does not require light to operate, but it is affected by light level.

Although ketamine–xylazine anesthesia has been used in visual experiments in rat (Girman & Lund, 2007), mouse (Sagdullaev & McCall, 2005), and cat (Haider et al., 2007), the question of whether or not it could induce the high-frequency oscillations seen here has not been engaged. Using a segment of data collected under urethane anesthesia over which the maintained discharge was stationary, it is clear that the high-frequency oscillations are still present (Fig. 7C, 7D). Both the multimodal interval histogram and the high frequency peak in the power

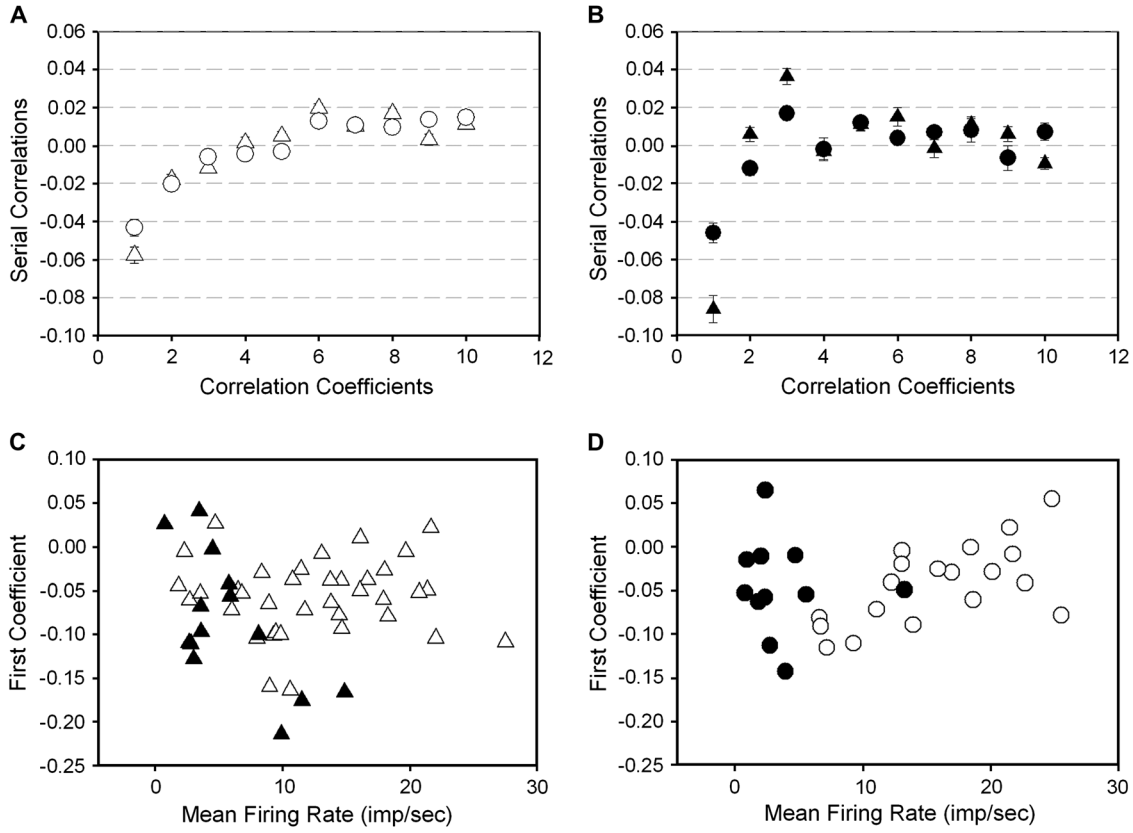

Fig. 4. Serial correlations among interspike intervals. The magnitude of serial coefficients 1–10 were averaged over all ON cells (**A**) and OFF cells (**B**) where all cells show negative first-order correlations and ON cells also showed significant second-order correlations ($P < 0.05$). The first correlation coefficient is plotted for all X cells (**C**) and Y cells (**D**) (ON-X, open triangles; ON-Y, open circles; OFF-X, filled triangles; OFF-Y, filled circles).

spectrum are features seen under both urethane and ketamine–xylazine anesthesia. It is therefore not likely that the oscillatory behavior is caused by the anesthetics.

Gamma-distributed intervals

A subset of rat ganglion cells (13 of 81) had maintained discharges that did not show multimodal interval histograms and oscillatory peaks in their power spectra. The interval histograms of these cells were fit well by a gamma distribution function:

$$f(\tau)=(\kappa/\mu)\tau^{\kappa-1}\exp(-\kappa\tau/\mu)/\Gamma(\kappa),$$

where τ is the independent variable of interspike intervals, μ is the mean interval, κ is the order of the gamma distribution, and $\Gamma(\kappa)$ is the gamma function evaluated at κ. Fig. 8A gives an example of such a cell, which has best-fit parameters of $\kappa = 3.01$ and $\mu = 98.20$. The distribution of best-fit κ and μ values on a cell-by-cell basis (Fig. 8B) shows a slight negative correlation ($r = -0.74$). This means that cells with higher mean firing rates and therefore a smaller mean interval, μ, are fit by higher order gamma functions and have narrower interval distributions.

If the maintained discharge was fully described by a gamma renewal process, then randomly shuffling the order of interspike intervals would not affect the power spectrum because the intervals would already be temporally uncorrelated. This was generally not the case. While the power spectra of maintained discharge before and after shuffling overlapped at most frequencies, there is a clear deviation at low frequencies (Fig. 8C), as also seen for some cat ganglion cells (Troy & Robson, 1992). The power spectrum that would result from a gamma renewal process with μ and κ determined by the best-fit interval distribution is indicated by the line in Fig. 8C. It follows the spectrum of the shuffled spike trains closely, indicating that the serial correlations among intervals in maintained discharge described earlier (Fig. 4) caused the low-frequency power density to depart slightly from that expected from a strict renewal process.

Modeling the maintained discharge

Studies have shown that a simple integrate-and-fire model with a white noise input produces simulated spike trains that have gamma-distributed intervals like those of cat retinal ganglion cells (Levine, 1991; Passaglia & Troy, 2004). We modified this model to account for the oscillatory behavior seen in most rat retinal ganglion cells. First, we considered the possible sources of this high-frequency energy. The simplest explanation is that the cell intrinsically fires spikes at intervals of ~30 ms. This would produce an oscillatory peak at the appropriate frequency in the power spectrum of the maintained discharge. The multimodal interval histograms, however, suggests that there is some oscillatory drive on the spike generator. The model was therefore modified to include a sinusoidal input.

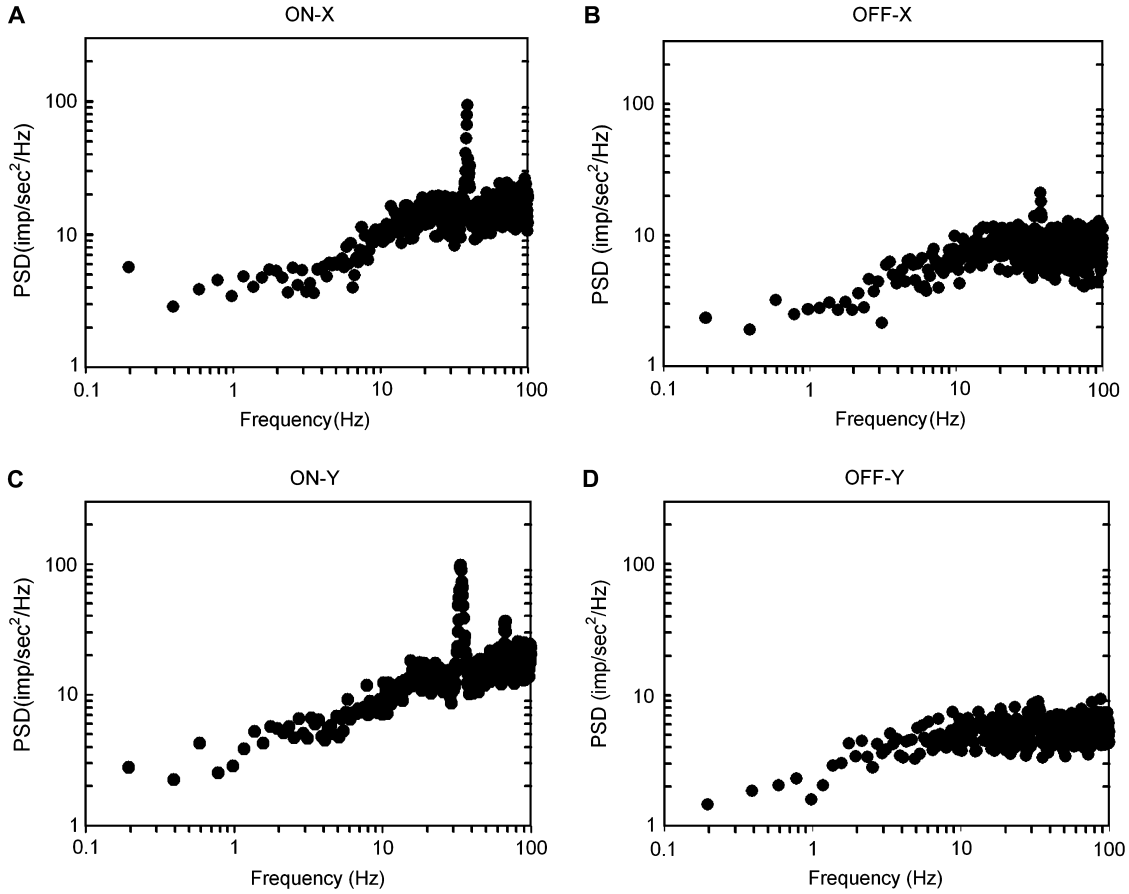

Fig. 5. Power spectral densities (PSD) of the spike trains are plotted for each cell type. The power density is flat at low frequencies and ramps up to a value equal to the mean rate of the cell. (**A**) ON-X cell (R81C2), mean rate: 16.1 impulses/s. (**B**) ON-Y cell (R77C4), mean rate: 18.6 impulses/s. (**C**) OFF-X cell (R92C11), mean rate: 8.1 impulses/s. (**D**) OFF-Y cell (R64C8), mean rate: 6.8 impulses/s. High frequency peaks are clearer in the ON cells (**A**, **C**) than the OFF cells (**B**, **D**). The unit of power density is in $(\text{impulses/s})^2$ per unit Hz.

An integrate-and-fire model was implemented with the output variable, $V(t)$, representing the membrane voltage of the cell. The differential equation was solved numerically using a second-order Runge–Kutta method in Matlab with a time step of 1 ms. When $V(t)$ reaches a given threshold, V_{th}, a spike is fired and the voltage is reset to a value of V_{reset}. The model equations are given by

$$\frac{\mathrm{d}V(t)}{\mathrm{d}t} = \mu + I_n(t) + I_{\text{osc}}(t),$$

where μ sets the mean firing rate of the model cell and $I_n(t)$ is the white noise that was generated by pulling independent values from a zero-mean Gaussian distribution with standard deviation σ, resulting in a bandwidth of 500 Hz. $I_{\text{osc}}(t)$ is a random-phase oscillatory drive on the spiking mechanism defined as

$$I_{\text{osc}}(t) = A\ \sin(2\pi f_{\text{osc}} t + \phi(t)),$$

where f_{osc} is the frequency of oscillation, A is the amplitude, and $\phi(t)$ is the random phase given by low bandwidth (<1 Hz), zero-mean Gaussian noise with standard deviation σ_{phase}. The noise signal $\phi(t)$ was generated in the same way as $I_n(t)$ but was then passed through a first-order lowpass filter with 1 Hz cutoff. The model output $V(t)$ without the oscillatory drive is shown in Fig. 9A. In this case, the Gaussian input noise causes jitter in the spike times that would otherwise occur at regular intervals and the result would be a unimodal gamma-distributed interval histogram. The addition of the oscillatory drive introduces subthreshold oscillations into the voltage record (Fig. 9B). The result is that the interval histogram now has multiple modes and can describe the interval and spectral data of a typical rat ganglion cell very well (Fig. 9B–9D).

This model also reproduced the small hump in interspike intervals in the range of 4–12 ms seen for many cells. A refractory period was not explicitly introduced because the integrative nature of the model eliminates very short intervals and effectively acts as a refractory period. Inspection of the spike trains confirmed that this hump in the interval histogram is caused by two spikes being occasionally fired during one cycle of the sinusoidal input. The absence of intervals in the range of 12–20 ms is due to the downward phase of the sinusoid moving $V(t)$ away from spike threshold.

Discussion

Our results demonstrate that the maintained discharge of rat retinal ganglion cells is similar in many respects to that of other mammals but different in important ways as well. The similarities

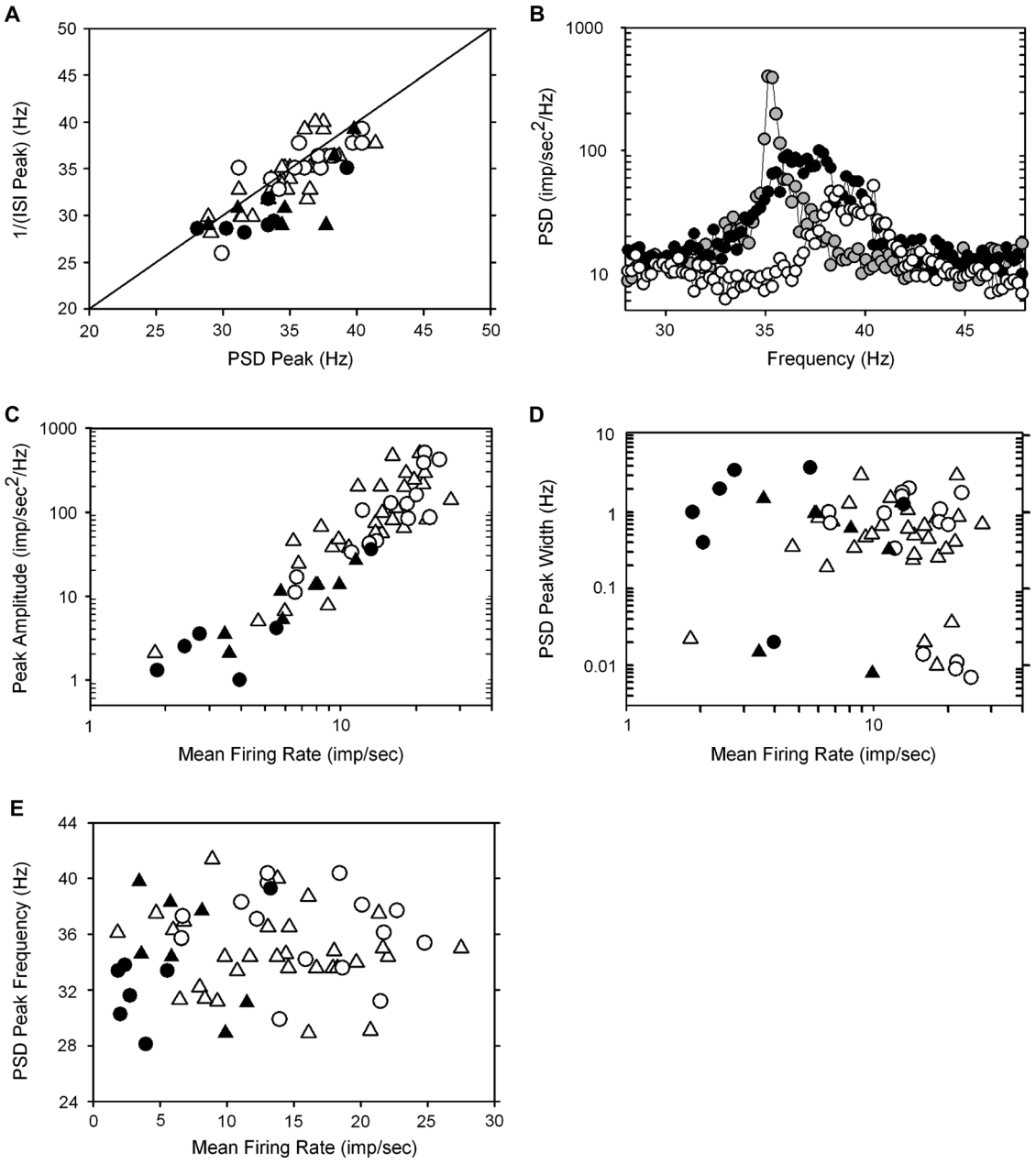

Fig. 6. Properties of the high frequency peak in the power spectral density (PSD). (**A**) The peak frequency of the PSD *versus* the inverse of the first peak of the interspike interval (ISI) distribution where the points are clustered around a line of unity slope ($r = 0.76$). (**B**) Zooming in on the high frequency peaks and plotting on a linear scale for three ON-Y cells, two of which are from the same animal (R94C2, white; R94C6, gray) and one from a separate animal (R92C1, black). The mean firing rate *versus* amplitude (**C**) and width (**D**) of the high frequency peak as well as *versus* the peak frequency (**E**). (ON-X, open triangles; ON-Y, open circles; OFF-X, filled triangles; OFF-Y, filled circles).

include higher firing rates in ON *versus* OFF cells, gamma-distributed interval statistics for some cells, and negative serial correlations between adjacent intervals for all cells. A major difference is that most rat retinal ganglion cells have a propensity for fast oscillatory discharge. The oscillations are characterized by multimodal interval distributions and high frequency peaks in power spectra that are rarely seen in other animals (Ogawa et al., 1966; Rodieck, 1967; Levine & Shefner, 1977). Another difference is that the maintained discharge properties of rat X and Y cells are not significantly different, whereas X cells tend to have higher mean rates than Y cells in cat (Troy & Robson, 1992).

Nonstationarity

The waxing and waning in maintained discharge reported here for rat retinal ganglion cells under urethane anesthesia has been observed in cat (Rodieck & Smith, 1966; Barlow & Levick, 1969) and ground squirrel (Tong, 1977). These studies considered the behavior pathological. Consistent with this interpretation, Kuffler et al.

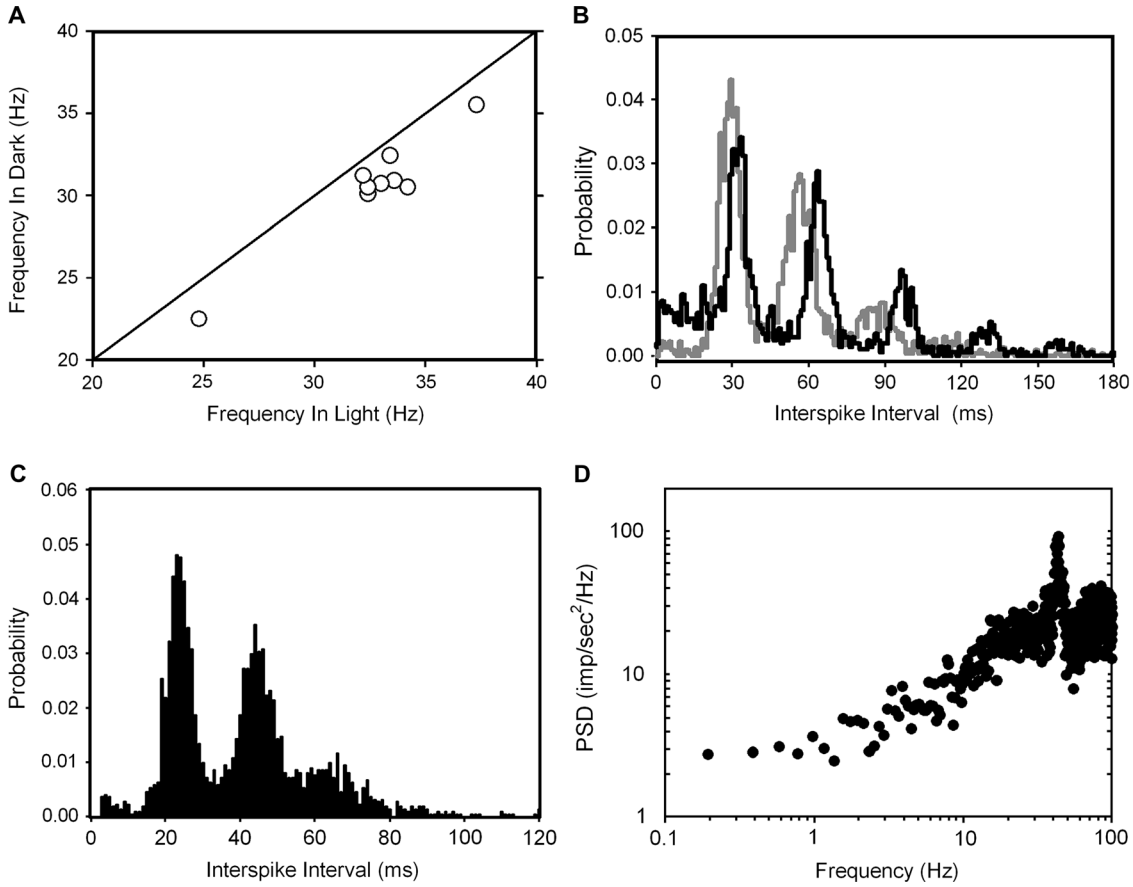

Fig. 7. Effect of urethane and light level on the high-frequency oscillations. (**A**) The frequency of the oscillations in the light *versus* the dark for nine ON cells with a line of unity slope, showing that the frequency decreased in the dark for all cells. (**B**) Interval distributions from an ON-X cell (R99C2) computed in the light (gray) and in the dark (black), showing that the peaks shift to slightly longer intervals in the dark. Collecting the maintained discharge under urethane anesthesia (R51C7) over a period in which the cell behaved stationary gave a multimodal interval distribution (**C**) and a power spectral density showing high-frequency oscillations (**D**) similar to the results under ketamine–xylazine anesthesia.

(1957) observed waxing and waning in cat intraocular recordings when pressure was exerted on a ganglion cell body, a clearly abnormal state. In order to rule out possible experimental variables, different rat strains, rat ages, and anesthetics were explored in this study. Interestingly, nonstationary behavior persisted for every condition except under ketamine–xylazine anesthesia, which suggests that the phenomenon might normally be present and ketamine–xylazine acts to abolish it. If this were the case though, it is unclear why waxing and waning was not noted in prior rat optic tract recordings that also used urethane (Brown & Rojas, 1965; Powers & Green, 1978; Cicerone & Green, 1980).

Interval and spike count statistics

The observed variability in both interspike intervals and spike counts is less for cells with higher mean firing rates. Thus, cells that fire more frequently tend to have a more regular discharge pattern, which is also seen in cat retinal ganglion cells (Troy & Robson, 1992). Interestingly, ON and OFF cells with similar firing rates tend to have similar discharge statistics, as evidenced by the tight overlap of points in Fig. 3. This implies that the observed variability in interspike intervals and spike counts is predicted by the mean firing rate of ON and OFF cells irrespective of cell polarity. In spite of their reported differences in intrinsic properties (Margolis & Detwiler, 2007), it would appear that the spiking mechanism and the noise that enters it are similar for ON and OFF cells since they produce the same statistics. If, for example, one cell type fired in a clocklike manner, then one would expect that for a given mean firing rate, the variability in intervals and spike counts would be very different for the two cell types.

High-frequency oscillations

Oscillatory mechanisms are known to exist within the mammalian retina. Evidence for their existence can be readily found in the electroretinogram (ERG) of most species (Frishman et al., 2000; Dong et al., 2004), including humans (Wachtmeister, 1998), in response to a light stimulus. The frequency of the oscillatory potential (OP) in rat depends on the amplitude of the stimulus, but even for weak stimuli, it is much faster (>60 Hz) than the oscillations we observe in the maintained discharge (Green & Kapousta-Bruneau, 1999; Hancock & Kraft, 2004). Oscillatory activity has also been seen in the subthreshold membrane potential fluctuations of retinal ganglion cells in cat (Przybyszewski et al., 1993) and mouse (Margolis & Detwiler, 2007). However, in both cases, the oscillatory strength was too weak to be observed in the spike train.

In spike recordings from cat, high-frequency oscillations are absent from X and Y cells (Troy & Robson, 1992), although

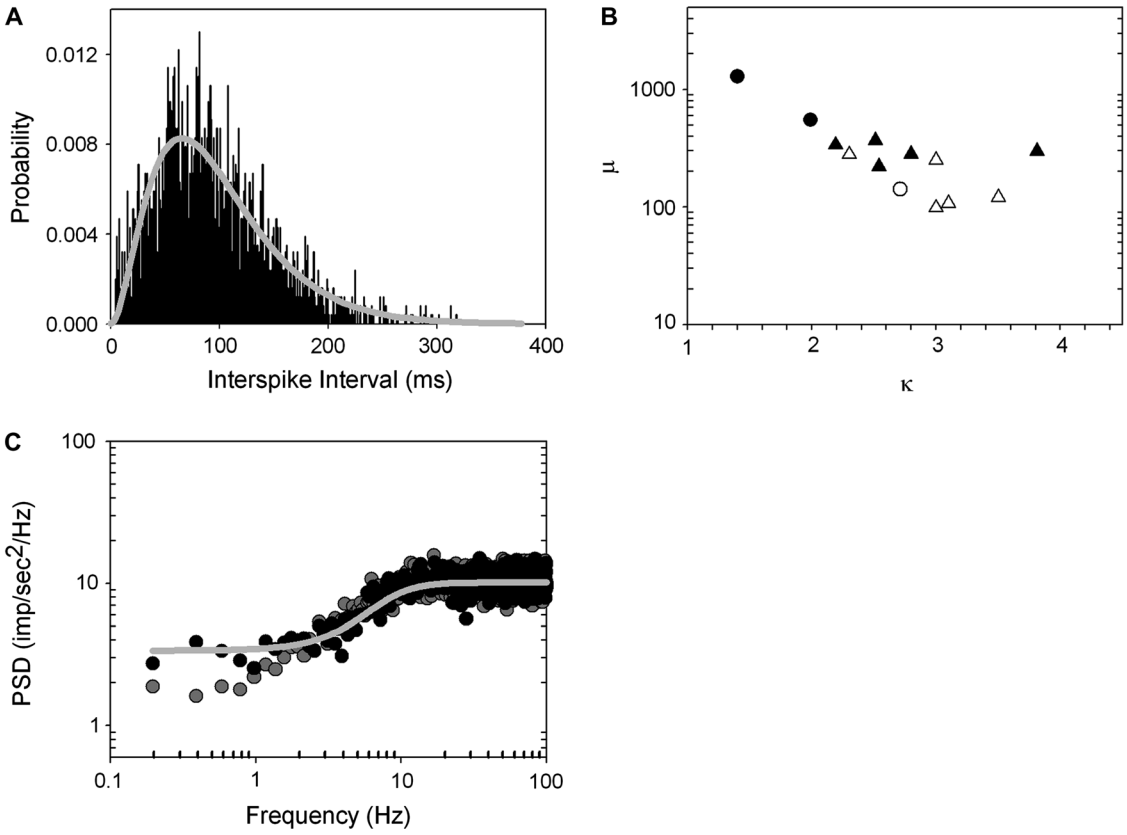

Fig. 8. Unimodal interspike interval distributions were fit well by a gamma distribution function. (**A**) The interval distribution for an ON-Y cell (R87C1) (black) and the best-fit gamma distribution function (gray line) ($\kappa = 3.0$ and $\mu = 98.2$). (**B**) The best-fit parameters κ and μ of the gamma distribution function for all cells with unimodal interval distributions show a negative correlation ($r = -0.74$) (ON-X, open triangles; ON-Y, open circles; OFF-X, filled triangles; OFF-Y, filled circles). (**C**) The power spectrum of the original spike train (gray dots) is plotted along with the spectrum of a spike train produced by randomly shuffling around the intervals (black dots) of the original spike train. The power spectrum that would have been predicted by a gamma renewal process with parameters determined by the best fit of the interval distribution is shown (gray line).

a clear peak in the power spectrum can be seen in the maintained discharge of Q cells (Robson & Troy, 1987), a less frequently encountered cat ganglion cell type. However, these oscillations are different from those observed here in that they result from the very regular discharge patterns of Q cells and not from an oscillatory drive on the ganglion cell. For example, a high-order gamma process will produce spikes at fairly regular intervals, which will result in a high frequency peak in the power spectrum. Alternatively, the multimodal interval distributions we observe can only be explained by the existence of some periodic forcing on the cell, which causes spikes to occur not just at a single preferred interval but at integer multiples of this preferred interval.

The retinal mechanism producing the oscillatory signal does not require light to operate since the fast oscillatory discharge persisted in darkness. That the oscillation frequency decreased slightly in the dark and was not completely independent of light suggests that it might serve a role in vision. The oscillation frequency may encode mean light level, although the change in oscillation frequency is small, so it could provide only a gross estimate of light level (e.g., scotopic or photopic regime). Other ganglion cell types, such as the so-called luminance units (Barlow & Levick, 1969; Troy et al., 1995) or intrinsically photosensitive ganglion cells (Dacey et al., 2005), may signal the illumination level via the mean firing rate of the cell, while the mean firing rates of X and Y cells are not thought to signal light level (Troy & Enroth-Cugell, 1993). Thus, changes in the oscillation frequency of X and Y cells provide an alternative method for signaling a dramatic change in light level.

The oscillations could also be involved in population encoding of global stimulus features (Kenyon et al., 2003; Ishikane et al., 2005; Stephens et al., 2006). This idea is supported by recordings from pairs of ganglion cells, which were shown to oscillate in synchrony under stimulus-specific conditions (Ariel et al., 1983; Neuenschwander & Singer, 1996; Neuenschwander et al., 1999). The synchronization was detectable from cell pairs more than 20 deg apart in visual angle and must therefore use laterally projecting amacrine or horizontal cells. However, the frequency of stimulus-induced oscillations (~85 Hz) was seen to be significantly different from that of oscillations in the maintained discharge (~30 Hz), suggesting that they may be separate phenomena. This would be consistent with the observation that light-induced OPs in the rat ERG are higher in frequency than the oscillations in the maintained discharge reported here. Whether these oscillations are synchronous between ganglion cells in the rat retina requires further examination using multiunit recordings.

The cellular origin of retinal oscillations is unclear, but there are arguments against an outer retinal component. If the photoreceptors themselves were the source, then their oscillatory outputs would all need to be in phase so that their signals do not cancel upon summation at the bipolar and ganglion cell levels.

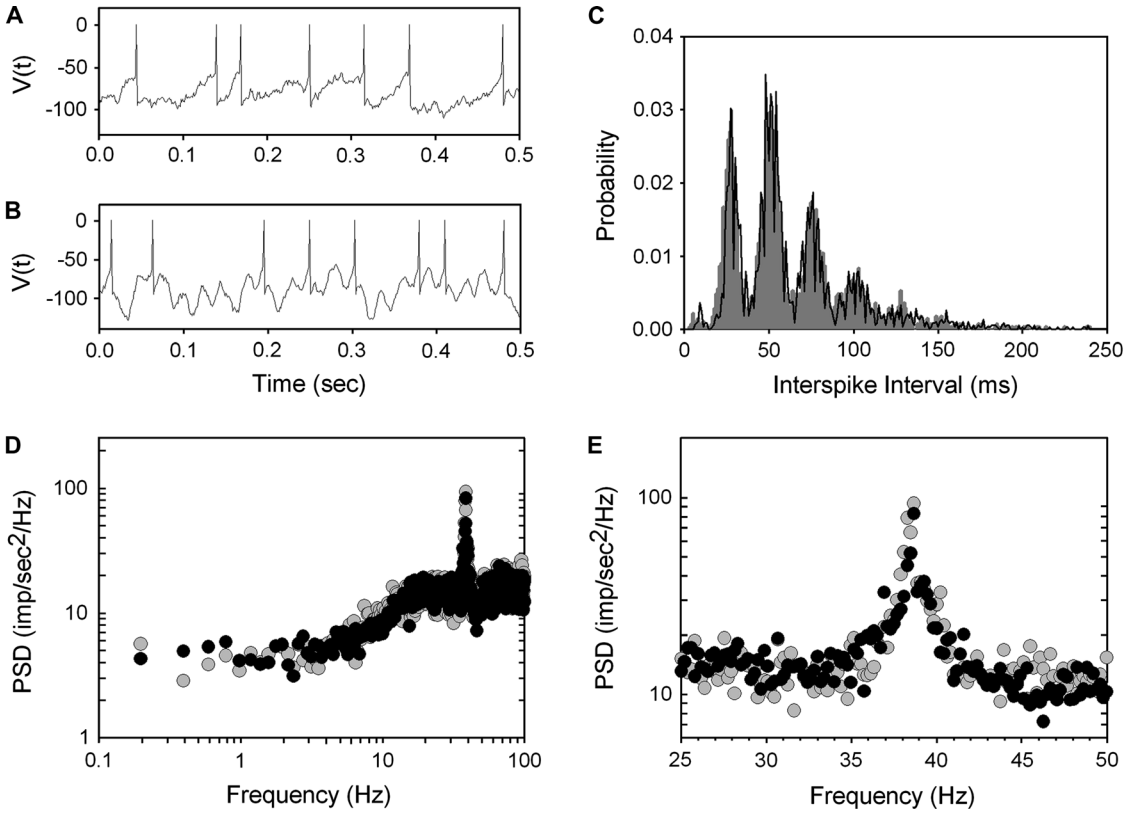

Fig. 9. Modified integrate-and-fire model. The output, $V(t)$, is shown for the case where $I_{osc} = 0$ (**A**) and for the case where there is an oscillatory drive (**B**). (**C**) The interval distribution of an example ON-X cell (R81C2) (gray) is shown along with the best-fit interval distribution of the model (black). (**D**) The corresponding power spectra of the spike trains that produced the interval distributions shown in **C**. The high frequency peak of the power spectrum is zoomed in and plotted on a linear scale (**E**). The best-fit parameters are $f_{osc} = 38.6$, $\mu = 710$, $\sigma = 2650$, $\sigma_{phase} = 29$, $A = 3750$, $V_{th} = -55$, and $V_{reset} = -95$.

While it is conceivable that neighboring photoreceptors communicating by gap junctions could oscillate in phase, the number of photoreceptors that converge onto an individual ganglion cell in the rat retina is large (Mayhew & Astle, 1997), which would make it difficult for the photoreceptors separated by large distances to oscillate in phase. Horizontal cells have been shown to oscillate under certain conditions (Foerster et al., 1977), but the oscillations are not thought to reach ganglion cells (Przybyszewski et al., 1993). The source most likely resides in the inner retina, where certain types of amacrine cells are known to oscillate both in the dark and in response to light (Sakai & Naka, 1988; Vigh et al., 2003). Or it could be an intrinsic property of the ganglion cell membrane, though such an explanation could only account for our data and not the long-range synchronous oscillations reported in cat (Neuenschwander et al., 1999).

Modeling

The wide bandwidth of the high frequency peak in the power spectrum of most cells was captured by the model by assuming that the oscillatory drive has stochastic phase. It was necessary to modulate the phase on a much slower timescale than the oscillation frequency in order for the waveform to still resemble a sinusoid. If a pure sinusoid was used for the oscillatory driving force, the resulting spike train had a spectrum with an extremely narrow high frequency peak. It was possible to incorporate an array of pure sinusoids closely spaced in frequency in order to fit the data, but such a model seemed less physiologically plausible than the random-phase model.

Although the interspike interval distributions can be classified as being multimodal or gamma in shape, they are not completely distinct from a functional perspective. As the model demonstrates, multimodal interval distributions arise naturally from a gamma process by introducing an oscillatory driving force. Another interesting observation concerning the model is the extent to which the subthreshold membrane potential [$V(t)$] is dominated by the oscillatory driving force. The large amplitude of the oscillatory input was necessary to fit the data, suggesting that the high-frequency oscillations are a dominant force in governing rat retinal ganglion cell function.

Acknowledgments

We thank Dr. Dan Green for providing helpful technical input during the preparation of this article. This work was supported by NIH Grant R01-EY016849A and the Smith Family New Investigator Award.

References

Ariel, M., Daw, N.W. & Rader, R.K. (1983). Rhythmicity in rabbit retinal ganglion cell responses. *Vision Research* **23**, 1485–1493.

Barlow, H.B. & Levick, W.R. (1969). Changes in the maintained discharge with adaptation level in the cat retina. *Journal of Physiology* **202**, 669–718.

Bendat, J.S. & Piersol, A.G. (1986). *Random Data: Analysis and Measurement Procedures*, 2nd edition. New York: John Wiley and Sons.

Brainard, D.H. (1997). The psychophysics toolbox. *Spatial Vision* **10**, 433–436.

Brown, J.E. & Rojas, J.A. (1965). Rat retinal ganglion cell: Receptive field organization and maintained activity. *Journal of Neurophysiology* **28**, 1073–1090.

Cicerone, C.M. & Green, D.G. (1980). Light adaptation within the receptive centre of rat retinal ganglion cells. *Journal of Physiology* **301**, 517–534.

Cleland, B.G. & Levick, W.R. (1974). Brisk and sluggish concentrically organized ganglion cells in the cat's retina. *Journal of Physiology* **240**, 421–456.

Dacey, D.M., Liao, H.W., Peterson, B.B, Robinson, F.R., Smith, V.C., Pocorny, J., Yau, K.W. & Gamlin, P.D., (2005). Melanopsin-expressing ganglion cells in primate retina signal colour and irradiance and project to the LGN. *Nature* **433**(7027), 749–754.

Demb, J.B., Sterling, P. & Freed, M.A. (2004). How retinal ganglion cells prevent synaptic noise from reaching the spike output. *Journal of Neurophysiology* **92**, 2510–2519.

Dong, C.J., Agey, P. & Hare, W.A. (2004). Origins of the electroretinogram oscillatory potentials in the rabbit retina. *Visual Neuroscience* **21**, 533–543.

Foerster, M.H., van de Grind, W.A. & Grusser, O.-J. (1977). Frequency transfer properties of three distinct types of cat horizontal cells. *Experimental Brain Research* **29**, 347–366.

Freed, M.A. (2005). Quantal encoding of information in a retinal ganglion cell. *Journal of Neurophysiology* **94**, 1048–1056.

Frishman, L.J. & Levine, M.W. (1983). Statistics of the maintained discharge of cat retinal ganglion cells. *Journal of Physiology* **339**, 475–494.

Frishman, L.J., Saszik, S., Harwerth, R.S., Viswanathan, S., Li, Y., Smith, E.L., III, Robson, J.G. & Barnes, G. (2000). Effects of experimental glaucoma in macaques on the multifocal ERG. Multifocal ERG in laser-induced glaucoma. *Documenta Ophthalmologica* **100**, 231–251.

Girman, S.V. & Lund, R.D. (2007). Most superficial sublamina of rat superior colliculus: Neuronal response properties and correlates with perceptual figure-ground segregation. *Journal of Neurophysiology* **98**, 161–177.

Goldberg, J.M., Adrian, H.O. & Smith, F.D. (1964). Response of neurons of the superior olivary complex of the cat to acoustic stimuli of long duration. *Journal of Neurophysiology* **27**, 706–749.

Green, D.G. & Kapousta-Bruneau, N.V. (1999). Electrophysiological properties of a new isolated rat preparation. *Vision Research* **39**, 2165–2177.

Haider, B., Duque, A., Hasenstaub, A.R., Yu, Y. & McCormick, D.A. (2007). Enhancement of visual responsiveness by spontaneous local network activity *in vivo*. *Journal of Neurophysiology* **97**, 4186–4202.

Hancock, H.A. & Kraft, T.W. (2004). Oscillatory potential analysis and ERGs of normal and diabetic rats. *Investigative Ophthalmology and Visual Science* **45**, 1002–1008.

Hecht, S., Schlaer, S. & Pirenne, M.H. (1942). Energy, quanta, and vision. *Journal of General Physiology* **25**, 819–840.

Hochstein, S. & Shapley, R.M. (1976). Linear and nonlinear spatial subunits in Y cat retinal ganglion cells. *Journal of Physiology* **262**, 265–284.

Ishikane, H., Gangi, M., Honda, S. & Tachibana, M. (2005). Synchronized retinal oscillations encode essential information for escape behavior in frogs. *Nature Neuroscience* **8**, 1087–1095.

Kenyon, G.T., Moore, B., Jeffs, J., Denning, K.S., Stephens, G.J., Travis, B.J., George, J.S., Theiler, J. & Marshak, D.W. (2003). A model of high-frequency oscillatory potentials in retinal ganglion cells. *Visual Neuroscience* **20**, 465–480.

Kuffler, S.W., Fitzhugh, R. & Barlow, H.B. (1957). Maintained activity in the cat's retina in light and darkness. *Journal of General Physiology* **40**, 683–702.

Levick, W.R. (1972). Another tungsten microelectrode. *Medical and Biological Engineering* **10**, 510–515.

Levick, W.R. & Williams, W.O. (1964). Maintained activity of lateral geniculate neurones in darkness. *Journal of Physiology* **170**, 582–597.

Levine, M.W. (1991). The distribution of the intervals between neural impulses in the maintained discharges of retinal ganglion cells. *Biological Cybernetics* **65**, 459–467.

Levine, M.W. & Shefner, J.M. (1977). A model for the variability of interspike intervals during sustained firing of a retinal neuron. *Biophysical Journal* **19**, 241–252.

Margolis, D.J. & Detwiler, P.B. (2007). Different mechanisms generate maintained activity in ON and OFF retinal ganglion cells. *Journal of Neuroscience* **27**, 5594–6005.

Marmarelis, P.Z. & Marmarelis, V.Z. (1978). *Analysis of Physiological Systems. The White Noise Approach*. New York: Plenum Press.

Mayhew, T.M. & Astle, D. (1997). Photoreceptor number and outer segment disk membrane surface area in the retina of the rat: Stereological data for whole organ and average photoreceptor cell. *Journal of Neurocytology* **26**, 53–61.

Neuenschwander, S., Castelo-Branco, M. & Singer, W. (1999). Synchronous oscillations in the cat retina. *Vision Research* **39**, 2485–2497.

Neuenschwander, S. & Singer, W. (1996). Long-range synchronization of oscillatory light responses in the cat retina and lateral geniculate nucleus. *Nature* **379**, 728–733.

Ogawa, T., Bishop, P.O. & Levick, W.R. (1966). Temporal characteristics of responses to photopic stimulation by single ganglion cells in the unopened eye of the cat. *Journal of Neurophysiology* **29**, 1–30.

Passaglia, C.L. & Troy, J.B. (2004). Impact of noise on retinal coding of visual signals. *Journal of Neurophysiology* **92**, 1023–1033.

Perkel, D.H., Gerstein, G.L. & Moore, G.P. (1967). Neuronal spike trains and stochastic point processes. I. The single spike train. *Biophysical Journal* **7**, 391–418.

Powers, M.K. & Green, D.G. (1978). Single retinal ganglion cell responses in the dark-reared rat: Grating acuity, contrast sensitivity, and defocusing. *Vision Research* **18**, 1533–1539.

Przybyszewski, A.W., Lankheet, M.J.M. & Van De Grind, W.A. (1993). Nonlinearity and oscillations in X-type ganglion cells of the cat retina. *Vision Research* **7**, 861–875.

Robson, J.G. & Troy, J.B. (1987). Nature of the maintained discharge of Q, X, and Y retinal ganglion cells of the cat. *Journal of the Optical Society of America A* **4**, 2301–2307.

Rodieck, R.W. (1967). Maintained activity of cat retinal ganglion cells. *Journal of Neurophysiology* **30**, 1043–1071.

Rodieck, R.W. & Smith, P.S. (1966). Slow dark discharge rhythms of cat retinal ganglion cells. *Journal of Neurophysiology* **29**, 942–953.

Sagdullaev, B.T. & McCall, M.A. (2005). Stimulus size and intensity alter fundamental receptive field properties of mouse retinal ganglion cells *in vivo*. *Visual Neuroscience* **22**, 649–659.

Sakai, H.M. & Naka, K. (1988). Dissection of the neuron network in the catfish inner retina. I. Transmission to ganglion cells. *Journal of Neurophysiology* **60**, 1549–1567.

Schneeweis, D.M. & Schnapf, J.L. (1999). The photovoltage of macaque cone photoreceptors: Adaptation, noise, and kinetics. *Journal of Neuroscience* **19**, 1203–1216.

Stephens, G.J., Neuenschwander, S., George, J.S., Singer, W. & Kenyon, G.T. (2006) See globally, spike locally: Oscillations in a retinal model encode large visual features. *Biological Cybernetics* **95**, 327–348.

Teich, M.B., Heneghan, C., Lowen, S.B., Ozaki, T. & Kaplan, E. (1997). Fractal character of the neural spike train in the visual system of the cat. *Journal of the Optical Society of America A* **14**, 529–546.

Tong, L. (1977). Contrast sensitive and color opponent optic tract fibers in the Mexican ground squirrel. Ph.D. Thesis, University of Michigan.

Troy, J.B. & Enroth-Cugell, C. (1993). X and Y ganglion cells inform the cat's brain about contrast in the retinal image. *Experimental Brain Research* **93**, 383–390.

Troy, J.B. & Lee, B.B. (1994). Steady discharges of macaque retinal ganglion cells. *Visual Neuroscience* **11**, 111–118.

Troy, J.B. & Robson, J.G. (1992). Steady discharges of X and Y retinal ganglion cells of cat under photopic illuminance. *Visual Neuroscience* **9**, 535–553.

Troy, J.B., Schweitzer-Tong, D.E. & Enroth-Cugell, C. (1995). Receptive field properties of Q retinal ganglion cells of cat. *Visual Neuroscience* **12**, 285–300.

Troy, J.B. & Shou, T. (2002). The receptive fields of cat retinal ganglion cells in physiological and pathological states: Where we are after a half century of research. *Progress in Retinal and Eye Research* **21**, 263–302.

Vigh, J., Solessio, E., Morgans, C.W. & Lasater, E.M. (2003). Ionic mechanisms mediating oscillatory membrane potentials in wide-field retinal amacrine cells. *Journal of Neurophysiology* **90**, 431–443.

Wachtmeister, L. (1998). Oscillatory potentials in the retina: What do they reveal? *Progress in Retinal and Eye Research* **17**, 485–521.